Inorg. Chem. **2003**, *42*, 4918–4929

X-ray Structures, Photophysical Characterization, and Computational Analysis of Geometrically Constrained Copper(I)–Phenanthroline Complexes

John Cody,[†] Jeanette Dennisson,[†] Joshua Gilmore,[†] Donald G. VanDerveer,[†] Maged M. Henary,[†] Alan Gabrielli,[†] C. David Sherrill,*[,†] Yiyun Zhang,[‡] Chia-Pin Pan,[‡] Clemens Burda,*[,‡] and Christoph J. Fahrni*[,†]

School of Chemistry and Biochemistry, Georgia Institute of Technology, 770 State Street, Atlanta, Georgia 30332, and Center for Chemical Dynamics, Department of Chemistry, Case Western Reserve University, 10900 Euclid Avenue, Cleveland, Ohio 44106

Received May 16, 2003

A series of three geometrically constrained C_2-symmetric Cu(I) mono-phenanthroline complexes were characterized by X-ray structural analysis, and their photophysical properties were investigated by absorption and emission spectroscopy. Visible light excitation yielded metal-to-ligand charge-transfer (MLCT) excited states with luminescence lifetimes up to 155 ns. Ultrafast transient absorption spectroscopy provided further insights into the excited-state dynamics and suggests for all three complexes the formation of a phenanthroline radical anion. In agreement with electrochemical measurements, the data further indicate that coordinative rearrangements are involved in nonradiative deactivation of the excited states. According to time-dependent density functional theory calculations (B3LYP/6-31G**), the major MLCT transitions are polarized along the C_2 axis of the complex and originate predominantly from the copper d_{xz} orbital. The computational analysis identifies an excited-state manifold with a number of close-lying, potentially emissive triplet states and is in agreement with the multiexponential decay kinetics of the MLCT luminescence. The relationship between structural and photophysical data of the studied Cu(I) mono-phenanthroline complexes agrees well with current models describing the photophysics of the related Cu(I) bis-diimine complexes.

Introduction

Photoluminescent metal complexes with low-lying metal-to-ligand charge-transfer (MLCT) excited states have been extensively studied as chemical sensors, catalysts for solar energy conversion, or components in display devices.[1−5] The majority of work has focused on complexes of polypyridine or phenanthroline ligands in combination with second- or third-row transition elements with d^6 electron configuration, such as ruthenium(II), rhenium (I), or iridium(III).[6] In search for more cost-effective alternatives, copper-based systems have received increased attention over the past two decades.[7,8] In particular, copper(I) complexes of phenanthroline derivatives exhibit a strong metal-to-ligand charge-transfer absorption in the visible range, although the emission properties are typically compromised by short excited-state lifetimes and low quantum yields. Several detailed studies have shown that the two major nonradiative deactivation pathways are due to flattening distortion and exciplex quenching of the excited state in polar donor solvents.[9−12] Both pathways can

* Corresponding authors. E-mail: fahrni@chemistry.gatech.edu (C.J.F.); sherrill@chemistry.gatech.edu (C.D.S); cxb77@cwru.edu (C.B.).
[†] Georgia Institute of Technology.
[‡] Case Western Reserve University.

(1) Czarnik, A. W. *Fluorescent Chemosensors for Ion and Molecular Recognition*; American Chemical Society: Washington, DC, 1993.
(2) Lakowicz, J. R. *Topics in Fluorescence Spectroscopy. Volume 4: Probe Design and Chemical Sensing*; Plenum Press: New York, 1994.
(3) Chanon, M. *Homogeneous Photocatalysis*; Wiley & Sons: Chichester, 1997; Vol. 2.
(4) Roundhill, D. M. *Photochemistry and Photophysics of Metal Complexes*; Plenum Press: New York, 1994.
(5) Mauch, R. H.; Gumlich, H.-E. *Inorganic and Organic Electroluminescence*; Wissenschaft und Technik Verlag: Berlin, 1996.
(6) Kalyanasundaram, K. *Photochemistry of Polypyridine and Porphyrin Complexes*; Academic Press: London, 1997.
(7) Armaroli, N. *Chem. Soc. Rev.* **2001**, *30*, 113.
(8) McMillin, D. R.; McNett, K. M. *Chem. Rev.* **1998**, *98*, 1201.
(9) Eggleston, M. K.; McMillin, D. R.; Koenig, K. S.; Pallenberg, A. J. *Inorg. Chem.* **1997**, *36*, 172.
(10) Eggleston, M. K.; Fanwick, P. E.; Pallenberg, A. J.; McMillin, D. R. *Inorg. Chem.* **1997**, *36*, 4007.

10.1021/ic034529j CCC: $25.00
Published on Web 07/18/2003

be rationalized by the increased formal charge on the copper in the emissive CT state, which is stabilized by a square planar or five-coordinate coordination environment. Bulky substituents in the 2- and 9-positions of the phenanthroline ring greatly improve the quantum yield by both inhibiting flattening distortion and suppressing ligand-addition reactions in the excited state.

Luminescent copper(I) phenanthroline complexes might be suitable as highly specific luminescent probes for copper itself. All previously characterized luminescent Cu(I) phenanthroline complexes are based on homo- or heteroleptic systems (**A**) with 2:1 stoichiometry and pseudotetrahedral geometry.[7] Since a mixed-ligand environment complicates

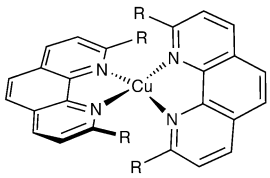

A

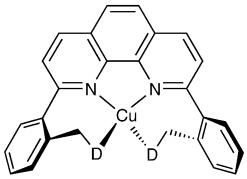

B

quantitative measurements, a 1:1 stoichiometry between analyte and ligand receptor would be preferable. Principally, a 1:1 complex stoichiometry can be achieved either by linking two phenanthroline moieties together or by attaching two additional donor groups (D) to a single phenanthroline core as shown in structure **B**. Molecular modeling studies of type **B** complexes suggest that the steric requirements of the 2-tolyl-donor substituents enforce a C_2-symmetric complex with a pseudotetrahedral coordination geometry.

The rigid ligand framework imposed by the biaryl-type linker in complex **B** is expected to reduce the previously mentioned nonradiative deactivation processes such as flattening distortion or exciplex quenching by the solvent. The following study describes the synthesis, structure, and photophysical characterization of three complexes of type **B** with various donor groups. As revealed by steady-state and time-resolved emission spectroscopy, the structural differences significantly affect their photophysical properties. Time-dependent density functional calculations were performed to gain further insights into possible excited-state deactivation processes.

Experimental Section

Materials and Reagents. 2,9-Dichloro-[1,10]phenanthroline (**4**) was prepared according to a published procedure.[13] (2-Bromomethylphenyl)-boronic acid pinacol ester (Combiblock), pyrazole (Alfa Aesar, 98%), dimethyl pyrazole (Alfa Aesar, 99%), ethanethiol (Acros, 99%), $Pd(PPh_3)_4$ (Aldrich, 99%). NMR: δ in ppm vs $SiMe_4$ (0 ppm, ^{1}H, 300 MHz). MS: selected peaks; *m*/*z*. Melting points are uncorrected. Flash chromatography (FC): Merck silica gel (70−230 mesh). TLC: 0.25 mm, Merck silica gel 60 F_{254}, visualizing at 254 nm or with 2% $KMnO_4$ solution.

Synthesis: (a) 2-(2-Ethylsulfanylmethyl-phenyl)-4,4,5,5-tetramethyl-[1,3,2]dioxaborolane (2). A solution of ethanethiol (270 μL, 0.81 mmol) and sodium hydroxide (80 mg) in 4.0 mL of ethanol was added dropwise to a solution of (2-bromomethylphenyl)boronic acid pinacol ester (200 mg, 0.67 mmol) in 4.0 mL of ethanol. After the reaction mixture was stirred for 30 min at room temperature, the solvent was evaporated and the residue purified by column chromatography on silica gel (20:1 hexane/EtOAc) to yield 100 mg (54%) of pinacol ester **2** as a colorless oil. R_f: 0.25 (30:1 hexane/EtOAc). ^{1}H NMR ($CDCl_3$, 300 MHz): δ 1.20 (t, J = 7.1 Hz, 3H), 1.35 (s, 12H), 2.40 (t, J = 7.1 Hz, 2H), 4.03 (s, 2H), 7.21 (td, J = 7.1, 1.1 Hz, 1H), 7.25 (d, J = 7.1 Hz, 1H), 7.33 (dd, J = 7.7, 1.6 Hz, 1H), 7.78 (dd, J = 7.1, 1.6 Hz, 1H). MS (EI): *m*/*z* 278 (M^+, 37), 217 (35), 191 (32), 149 (73), 59 (42), 40 (100). FAB-HRMS: *m*/*e* calcd for (M + H) $C_{15}H_{23}BO_2S$ 278.2202, found 278.1512.

(b) 1-[2-(4,4,5,5-Tetramethyl-[1,3,2]dioxaborolan-2-yl)benzyl]-1*H*-pyrazole (3a). A mixture of pyrazole (950 mg, 14.0 mmol), sodium hydride (95 mg, 60% dispersion in mineral oil), and (2-bromomethylphenyl)boronic acid pinacol ester (500 mg, 1.68 mmol) in 5 mL of anhydrous dimethylformamide (DMF) was heated at 80 °C for 3 h. The solvent was removed under reduced pressure and the residue diluted with water and extracted twice with EtOAc. The combined organic layers were dried with $MgSO_4$ and concentrated under reduced pressure. The crude product was purified on silica gel (4:1 hexane/EtOAc) providing 185 mg (0.65 mmol, 39%) of boron ester **3a** as a colorless oil. R_f: 0.51 (1:1 hexane/EtOAc). ^{1}H NMR ($CDCl_3$, 300 MHz): δ 1.35 (s, 12H), 5.66 (s, 2H), 6.25 (t, J = 2.2 Hz, 1H), 7.01 (d, J = 7.7 Hz, 1H), 7.28 (td, J = 7.7, 1.1 Hz, 1H), 7.38 (td, J = 7.0, 1.6 Hz, 1H), 7.44 (d, J = 2.2 Hz, 1H), 7.55 (d, J = 1.1 Hz, 1H); 7.86 (dd, J = 7.1, 1.6 Hz, 1H). MS (EI): *m*/*z* 284 (M^+, 43), 225 (55), 184 (100), 117 (36). FAB-HRMS: *m*/*e* calcd for (M^+) $C_{16}H_{21}BN_2O_2$ 284.1696, found 284.1709.

(c) 3,5-Dimethyl-1-[2-(4,4,5,5-tetramethyl-[1,3,2]dioxaborolan-2-yl)-benzyl]-1*H*-pyrazole (3b) was synthesized as described for **3a**. Yield: 60%. R_f: 0.58 (2:1 hexane/EtOAc). ^{1}H NMR ($CDCl_3$, 300 MHz): δ 1.35 (s, 12H), 2.11 (s, 3H), 2.27 (s, 3H), 5.59 (s, 2H), 5.87 (s, 1H), 6.56 (d, J = 7.7 Hz, 1H), 7.20 (td, J = 7.1, 1.1 Hz, 1H), 7.31 (td, J = 7.7, 1.6 Hz, 1H), 7.85 (dd, J = 7.1, 1.6 Hz, 1H). MS (EI) *m*/*z* 313 (M^+, 13), 297 (93), 253 (33), 235 (36), 212 (100), 117 (38), 109 (51). FAB-HRMS: *m*/*e* calcd for (M^+) $C_{18}H_{26}BN_2O_2$ 313.2087, found 313.2104.

(d) 2,9-Bis-(2-ethylsulfanylmethyl-phenyl)-[1,10]phenanthroline (5). A solution of 2,9-dichloro-[1,10]phenanthroline (23 mg, 0.089 mmol), pinacol ester **2** (50 mg, 0.180 mmol), and a catalytic amount of tetrakis-triphenylphosphine palladium(0) (3 mg) in a mixture of 5 mL of ethanol and 5 mL of toluene was heated for 48 h at 120 °C in a sealed Schlenk tube under argon together with a solution of potassium carbonate (345 mg) in 5 mL of water. The reaction mixture was diluted with 10 mL of saturated NaCl and extracted twice with dichloromethane. The combined organic phase was dried ($MgSO_4$) and concentrated under reduced pressure. The residue was purified by flash chromatography on silica gel (1:1 hexane/ethyl acetate) to yield 32 mg (75%) of phenanthroline derivative **5** as a colorless solid. Mp: 117−118 °C. R_f: 0.47 (1:1 hexane/EtOAc). ^{1}H NMR ($CDCl_3$, 300 MHz): δ 0.98 (t, J = 14.8 Hz, 6H), 2.32 (q, J = 7.7 Hz, 4H), 4.40 (s, 2H), 7.33−7.37 (m, 4H), 7.48−7.51 (m, 2H), 7.57−7.60 (m, 2H), 7.83 (s, 2H), 7.91 (d, J = 8.2 Hz, 2H), 8.33 (d, J = 8.2 Hz, 2H). MS (EI): *m*/*z* 480 (M^+, 16), 419 (59), 389 (80), 357 (100), 178 (44). FAB-HRMS: *m*/*e* calcd for (M^+) $C_{30}H_{28}N_2S_2$ 480.1694, found 480.1694.

(11) Miller, M. T.; Gantzel, P. K.; Karpishin, T. B. *Inorg. Chem.* **1998**, *37*, 2285.
(12) Miller, M. T.; Gantzel, P. K.; Karpishin, T. B. *Inorg. Chem.* **1999**, *38*, 3414.
(13) Yamada, M.; Nakamura, Y.; Kuroda, S.; Shimao, I. *Bull. Chem. Soc. Jpn.* **1990**, *63*, 2710.

(e) 2,9-Bis-(2-pyrazol-1-ylmethyl-phenyl)-[1,10]phenanthroline (6a) was synthesized as described for **5**: Starting with 185 mg of boron ester **3a**, 57 mg of ligand **6a** was isolated as a colorless solid (34% yield). Mp: 188−190 °C. R_f: 0.27 (1:1 hexane/EtOAc). ^{1}H NMR ($CDCl_3$, 300 MHz): δ 5.72 (s, 4H), 5.78 (t, J = 4.4 Hz, 2H), 7.22−7.28 (m, 2H), 7.38−7.45 (m, 6H), 7.57−7.63 (m, 2H), 7.68 (d, J = 2.2 Hz, 2H), 7.82 (d, J = 8.2 Hz, 2H), 7.89 (s, 2H), 8.36 (d, J = 8.2 Hz, 2H). MS (FAB): m/z 493 (M^+, 43), 493 (100), 425 (33). FAB-HRMS: m/e calcd for $(M + H)^+$ $C_{32}H_{24}N_6$ 493.2141, found 493.2157.

(f) 2,9-Bis-[2-(3,5-dimethyl-pyrazol-1-ylmethyl)-phenyl][1,10]-phenanthroline (6b) was synthesized as described for **5**: Starting with 153 mg of boron ester **3b**, 80 mg of ligand **6b** was isolated as a colorless oil (30% yield). ^{1}H NMR ($CDCl_3$, 300 MHz): δ 1.88 (s, 6H), 2.17 (s, 6H), 5.68 (s, 4H), 5.73 (s, 2H), 6.73−6.76 (m, 2H), 7.30−7.38 (m, 4H), 7.59−7.65 (m, 2H), 7.86 (d, J = 8.2 Hz, 2H), 7.86 (s, 2H), 8.34 (d, J = 8.2 Hz, 2H). MS (FAB): 548 (M^+, 3), 452 (55), 356 (100). FAB-HRMS: m/e calcd for (M^+) $C_{36}H_{32}N_6$ 548.2675, found 548.2689.

(g) 2,9-Bis-(2-ethylsulfanylmethyl-phenyl)-[1,10]phenanthroline copper(I) hexafluorophosphate (7). A solution of phenanthroline derivative **5** (20 mg, 41 μmol) in 1 mL of acetonitrile was added dropwise to a solution of tetrakis(acetonitrile) copper(I) hexafluorophosphate (15.5 mg, 41 μmol). After stirring for 30 min at room temperature, the solvent was evaporated under reduced pressure and the residue recrystallized from dichloromethane/hexane affording 22.5 mg (32.6 μmol, 78%) of yellow crystals. Single crystals suitable for X-ray analysis were obtained from an acetonitrile solution of the complex by vapor diffusion with toluene. Mp: >300 °C. ^{1}H NMR ($CDCl_3$, 300 MHz): δ 0.74 (t, J = 7.4 Hz, 6H), 2.39 (q, J = 7.4 Hz, 4H), 3.32 (d, J = 11.5 Hz, 2H), 3.80 (d, J = 11.5 Hz, 2H), 7.39−7.41 (m, 2H), 7.51−7.61 (m, 6H), 8.07 (d, J = 8.2 Hz, 2H), 8.21 (s, 2H), 8.78 (d, J = 8.2 Hz, 2H). MS (FAB): m/z 543 (M^+, 100). FAB-HRMS: m/e calcd for (M^+) $C_{30}H_{28}CuN_2S_2$ 543.0989, found 543.0988.

(h) 2,9-Bis-(2-pyrazol-1-ylmethyl-phenyl)-[1,10]phenanthroline copper(I) hexafluorophosphate (8a) was synthesized from 2,9-bis-(2-pyrazol-1-ylmethyl-phenyl)-[1,10]phenanthroline **6a** as described for complex **7**. Yield: 78%, orange crystals. Single crystals suitable for X-ray analysis were obtained from an acetonitrile solution of the complex by vapor diffusion with toluene. Mp: >300 °C. ^{1}H NMR ($CDCl_3$, 300 MHz): δ 5.02−5.06 (AB multiplet, 4H), 5.54 (d, J = 2.2 Hz, 1H), 6.00 (t, J = 2.2 Hz, 2H), 7.58−7.67 (m, 8H), 8.13 (s, 2H), 8.16 (d, J = 8.2 Hz, 2H), 8.72 (d, J = 8.2 Hz, 2H). MS (FAB): m/z 555 (M^+, 100). FAB-HRMS: m/e calcd for (M^+) $C_{32}H_{24}N_6Cu$ 555.1358, found 555.1332.

(i) 2,9-Bis-[2-(3,5-dimethyl-pyrazol-1-ylmethyl)-phenyl][1,10]-phenanthroline copper(I) hexafluorophosphate (8b) was synthesized from 2,9-bis-[2-(3,5-dimethyl-pyrazol-1-ylmethyl)-phenyl]-[1,10]phenanthroline **6b** as described for complex **7**. Yield: 77%, red crystals. Single crystals suitable for X-ray analysis were obtained by vapor diffusion with toluene of an acetonitrile solution of the complex. Mp: >300 °C. ^{1}H NMR ($CDCl_3$, 300 MHz): δ 0.75 (s, 6H), 2.39 (s, 6H), 4.82−4.86 (AB multiplet, 4H), 5.68 (s, 2H), 7.17 (d, J = 7.14 Hz, 2H), 7.45−7.56 (m, 4H), 7.70 (d, J = 8.2 Hz, 2H), 8.05 (d, J = 8.2 Hz, 2H), 8.15 (s, 2H), 8.72 (d, J = 8.2 Hz, 2H). MS (FAB): m/z 611 (M^+, 100). FAB-HRMS: m/e calcd for (M^+) $C_{36}H_{32}N_6Cu$ 611.1984, found 611.1982.

Steady-State Absorption and Emission Spectroscopy. UV−vis absorption spectra were recorded at 25 °C using a Varian Cary Bio50 spectrometer with constant-temperature accessory. Steady-state emission and excitation spectra were recorded with a PTI fluorimeter. Quantum yields were determined using degassed dichloromethane with $[Ru(bpy)_3](PF_6)_2$ as standard (Φ_f (H_2O) = 0.042).[14]

Time-Resolved Emission Spectroscopy. Time-resolved emission was measured by time-correlated single photon counting. The excitation source was a Spectra-Physics (SP) Tsunami Ti-sapphire laser pumped with a SP Millennia diode-pumped Nd−YVO_4 laser. The repetition rate was set at 4 MHz with 2.2 ps pulse width. The output was frequency doubled by a SP GWU HG flexible harmonic generator and used as the excitation source. The emission was detected by a cooled Hamamatsu (Hamamatsu, Japan) R3809U-50 microchannel plate photomultiplier, while a SPC-330-12 PC module (Becker & Hickl GmbH Intelligent Measurement and Control Systems, Berlin, Germany) was used for the photon counting electronics. The excitation wavelength used was 390 nm, and the emission was monitored at 650 nm. Luminescence decays were acquired simultaneously with a lamp profile in 1024 channels of 9.8 ps/channel. Decay curves were deconvoluted using the Beechem global program.[15] Goodness of fit was judged by reduced chi-square, χ_r^2, and the autocorrelation function of the weighted residuals.

Transient Absorption Spectroscopy. Femtosecond time-resolved transient absorption measurements were recorded with a femtosecond laser system that has been previously described.[16] Samples were excited at 390 nm with a laser pulse of 120 fs duration (fwhm) and 0.8 mJ/cm^2 output energy per pulse. The excitation beam is focused to a spot diameter of about 500 μm and the probe beam to 100 μm. The samples were measured in a quartz cuvette of 2 mm path length and stirred by a cell stirrer to avoid permanent bleaching of the pump−probe volume element in the solution. All pump−probe experiments were carried out under ambient conditions.

Cyclic Voltammetry. The cyclic voltammograms were acquired in acetonitrile (freshly distilled from calcium hydride) containing 0.1 M Bu_4NPF_6 as electrolyte using a CH-Instruments potentiostat (model 600A). The samples were measured under inert gas at a concentration of 3 mM in a single compartment cell with Pt working and counter electrode and Ag/AgCl reference electrode. The half-wave potentials were referenced to ferrocene as internal standard, and the measurements were typically performed with a 100 mV s^{-1} scan rate.

Computational Methods. All computations were carried out using the Q-Chem electronic structure package.[17] Geometries of the electronic ground states were determined using density functional theory (DFT), applying the B3LYP method[18] which includes Becke's three-parameter hybrid exchange functional[19] and the gradient-corrected correlation functional of Lee, Yang, and Parr.[20] Computations employed the 6-31G** basis,[21,22] which is a valence double-ζ basis with d polarization functions on first-row atoms, p polarization on hydrogens, and f polarization on copper. Estimates

(14) Caspar, J. V.; Meyer, T. J. *J. Am. Chem. Soc.* **1983**, *105*, 5583.
(15) Beechem, J. M. *Chem. Phys. Lipids* **1989**, *50*, 237.
(16) Burda, C.; Samia, A. C. S.; Hathcock, D. J.; Huang, H. J.; Yang, S. *J. Am. Chem. Soc.* **2002**, *124*, 12400.
(17) Kong, J.; White, C. A.; Krylov, A. I.; Sherrill, D.; Adamson, R. D.; Furlani, T. R.; Lee, M. S.; Lee, A. M.; Gwaltney, S. R.; Adams, T. R.; Ochsenfeld, C.; Gilbert, A. T. B.; Kedziora, G. S.; Rassolov, V. A.; Maurice, D. R.; Nair, N.; Shao, Y. H.; Besley, N. A.; Maslen, P. E.; Dombroski, J. P.; Daschel, H.; Zhang, W. M.; Korambath, P. P.; Baker, J.; Byrd, E. F. C.; Van Voorhis, T.; Oumi, M.; Hirata, S.; Hsu, C. P.; Ishikawa, N.; Florian, J.; Warshel, A.; Johnson, B. G.; Gill, P. M. W.; Head-Gordon, M.; Pople, J. A. *J. Comput. Chem.* **2000**, *21*, 1532.
(18) Stephens, P. J.; Devlin, F. J.; Chabalowski, C. F.; Frisch, M. J. *J. Phys. Chem.* **1994**, *98*, 11623.
(19) Becke, A. D. *J. Chem. Phys.* **1993**, *98*, 1372.
(20) Lee, C. T.; Yang, W. T.; Parr, R. G. *Phys. Rev. B* **1988**, *37*, 785.

Table 1. Crystallographic Data for Complexes **7**, **8a**, and **8b**

	[Cu(bempp)]PF_6 (**7**)	[Cu(bpmpp)]PF_6 (**8a**)	[Cu(bdmpp)]PF_6 (**8b**)
formula	$C_{30}H_{28}CuF_6N_2PS_2$	$C_{33.5}H_{27}Cl_3CuF_6N_6P$	$C_{30}H_{32}CuF_6N_6P$
color, habit	yellow prisms	dark red prisms	dark red prisms
cryst size (mm)	0.25 × 0.14 × 0.03	0.24 × 0.17 × 0.07	0.44 × 0.37 × 0.27
cryst syst	monoclinic	triclinic	monoclinic
space group	*P*2(1)/*n*	$P\bar{1}$	*P*2(1)/*n*
a (Å)	12.740(2)	10.6375(13)	12.0457(18)
b (Å)	14.140(2)	12.7868(16)	9.3115(14)
c (Å)	16.198(3)	14.6402(18)	29.488(5)
α (deg)	90	109.599(2)	90
β (deg)	95.061(3)	111.207(2)	91.961(3)
γ (deg)	90	93.59(2)	90
V (Å^3)	2906.7(8)	1710.1(4)	3305.6(9)
Z	4	2	4
calcd density (g/cm^3)	1.575	1.609	1.521
F(000)	1408	838	1552
temp (K)	188(2)	198(2)	198(2)
2*θ* range (deg)	3.82−50.0	3.24−50.0	2.76−50.30
no. of reflns collected	15158	12921	23985
no. of indep reflns	5118	5989	5917
final *R* indices (obsd data) (%): *R*, R_w	5.16, 7.72	5.50, 14.11	3.73. 9.38
R indices (all data) (%): *R*, R_w	12.24, 9.27	8.38, 15.86	4.77, 10.29
GOF on F^2	0.910	1.044	1.064

of vertical excitation energies were obtained using time-dependent density functional theory (TD-DFT)[23,24] in the Tamm−Dancoff approximation[24] with the B3LYP functional and the 6-31G** basis at the ground-state optimized geometries. Molecular orbitals and electron attach/detach densities[25] were visualized with the MOLEKEL software[26] using the Q-Chem plot data. Details for all computations, including the coordinates of optimized geometries, are provided in the Supporting Information.

X-ray Structure Analysis. Crystals of complexes **7**, **8a**, and **8b** suitable for X-ray structural analysis were grown from acetonitrile−toluene by slow evaporation of the solvent over the period of several days. The X-ray data were collected on a Siemens SMART 1K CCD diffractometer with graphite-monochromated Mo Kα radiation ($\lambda = 0.71073$ Å). The program SADABS (Sheldrick)[27] and SAINT 6.22 (Bruker)[28] were used for absorption corrections. All structures were solved by direct methods and refined by least-squares calculations with the SHELXTL 5.10 software package.[28] The hydrogen atoms were added using ideal geometries with a fixed C−H bond distance of 0.96 Å. A summary of the crystallographic parameters and data is given in Table 1.

Results and Discussion

1. Synthesis. The three disubstituted phenanthroline ligands **5**, **6a**, and **6b** were synthesized via Suzuki cross coupling of 2,9-dichloro-[1,10]phenanthroline[13] **4** with the corresponding boron-picolinate as outlined in Scheme 1. Nucleophilic substitution of 2-bromomethylphenyl boron ester **1** with ethanethiol, pyrazole, or 2,4-dimethyl-pyrazole yielded the coupling partners **2**, **3a**, and **3b**. As reported by Bates and Parker[29] nucleophilic substitution of 2,9-bis-(2-bromomethyl-phenyl)-[1,10]phenanthroline results only in monosubstitution, and is accompanied by intramolecular cyclization of the second benzylic site to give a cationic N-alkylated product. Nucleophilic substitution of the bromomethyl group must therefore be carried out prior to the cross coupling reaction. The strategy is expected to be generally applicable to the synthesis of a wide variety of donor-substituted 2,9-diphenyl-[1,10]phenanthroline derivatives. Reaction of ligands **5**, **6a**, and **6b** with 1 molar equiv of $Cu(CH_3CN)_4$ provided the corresponding 1:1 complexes with good yield (78%).

2. Structural Studies. Crystal Structure of Cu(bempp)-PF_6 (7). Vapor diffusion of toluene into an acetonitrile solution of complex **7** yielded yellow crystals that were suitable for diffraction studies. An ORTEP view with atom-numbering scheme of the cation is given in Figure 1, and selected interatomic distances and angles are compiled in Table 2. As anticipated from initial molecular modeling studies, the copper center adopts a twisted tetrahedral coordination geometry that results in a pseudo-C_2 symmetry of the complex cation. With a dihedral angle of 74.1° between the N(1)−Cu−N(2) and S(1)−Cu−S(2) planes the coordination geometry deviates substantially from an ideal tetrahedral arrangement. The copper−sulfur bond distances Cu−S(1) and Cu−S(2) are 224 and 225 pm, respectively, and compare well with the distances of similar monovalent copper complexes of aliphatic sulfur donor ligands. For example, the tetrahedral complex bis(2,5-dithiahexane-*S*,*S*′′)-copper(I) perchlorate[30] exhibits a Cu−S distance of 226 pm, and an almost identical bond length of 225 pm was determined for the mixed sulfur−nitrogen donor ligand 1,5-dithia-9,13-diazacyclohexadecane.[31] Similarly, the copper−nitrogen bond lengths Cu−N(1) (206 pm) and Cu−N(2) (204 pm) compare well with the distances found for bis-phenan-

(21) Hariharan, P. C.; Pople, J. A. *Theor. Chim. Acta* **1973**, *28*, 213.
(22) Rassolov, V. A.; Pople, J. A.; Ratner, M. A.; Windus, T. L. *J. Chem. Phys.* **1998**, *109*, 1223.
(23) Bauernschmitt, R.; Ahlrichs, R. *Chem. Phys. Lett.* **1996**, *256*, 454.
(24) Hirata, S.; Head-Gordon, M. *Chem. Phys. Lett.* **1999**, *302*, 375.
(25) Head-Gordon, M.; Grana, A. M.; Maurice, D.; White, C. A. *J. Phys. Chem.* **1995**, *99*, 14261.
(26) Flükiger, P.; Lüthi, H. P.; Portmann, S.; Weber, J. *MOLEKEL*, v. 4.1; Swiss Center for Scientific Computing: Manno, 2000−2001.
(27) Blessing, R. H. *Acta Crystallogr., Sect. A* **1995**, *51*, 33.
(28) Bruker *AXS*: Madison, WI, 1998.
(29) Bates, G. B.; Parker, D. *Tetrahedron Lett.* **1996**, *37*, 267.
(30) Olmstead, M. M.; Musker, W. K.; Kessler, R. M. *Inorg. Chem.* **1981**, *20*, 151.
(31) Balakrishnan, K. P.; Riesen, A.; Zuberbühler, A. D.; Kaden, T. A. *Acta Crystallogr., Sect. C: Cryst. Struct. Commun.* **1990**, *46*, 1236.

Scheme 1

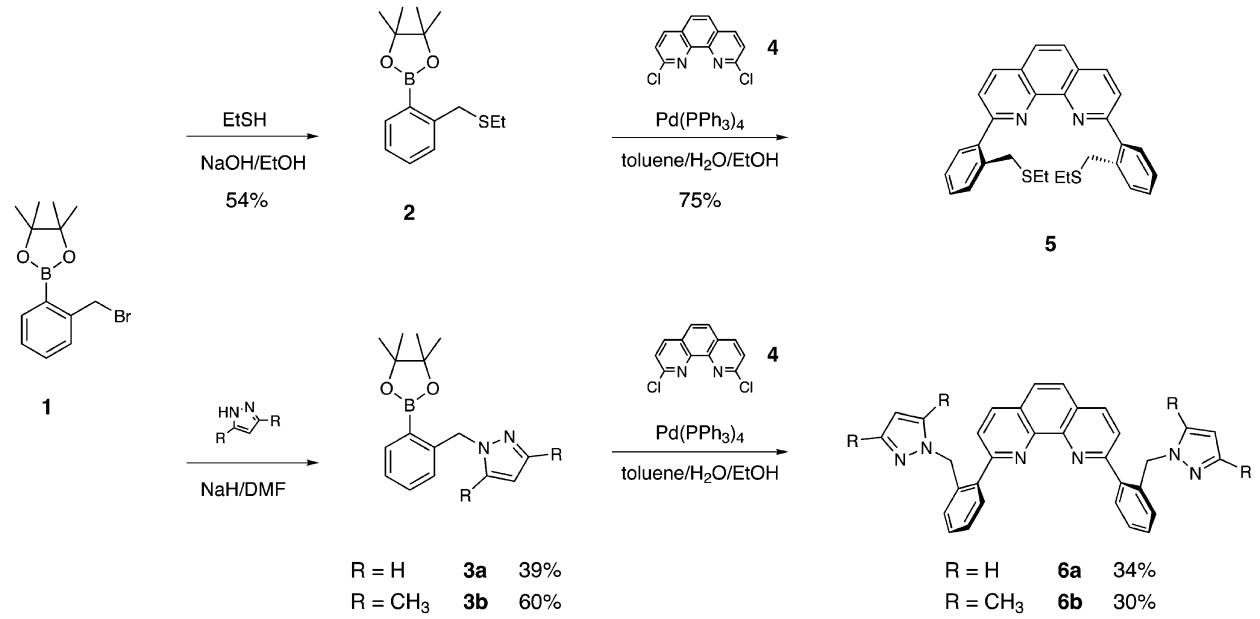

Table 2. Selected Experimental Structural Parameters for Cu(I) Complexes **7**, **8a**, and **8b**[a]

	[Cu(bempp)]PF_6 (**7**)		[Cu(bpmpp)]PF_6 (**8a**)	[Cu(bdmpp)]PF_6 (**8b**)
Cu(1)−N(1) (Å)	2.062(3)	Cu(1)−N(1) (Å)	2.046(4)	2.169(2)
Cu(1)−N(2) (Å)	2.044(4)	Cu(1)−N(2) (Å)	2.060(4)	2.091(2)
Cu(1)−S(1) (Å)	2.2397(13)	Cu(1)−N(3) (Å)	1.983(4)	2.042(2)
Cu(1)−S(2) (Å)	2.2544(13)	Cu(1)−N(5) (Å)	1.985(4)	2.061(2)
N(1)−Cu(1)−N(2) (deg)	81.90(14)	N(1)−Cu(1)−N(2) (deg)	81.74(14)	79.13(8)
N(1)−Cu(1)−S(1) (deg)	107.45(10)	N(1)−Cu(1)−N(3) (deg)	116.84(15)	113.20(8)
N(1)−Cu(1)−S(2) (deg)	121.59(10)	N(1)−Cu(1)−N(5) (deg)	118.62(15)	120.76(8)
N(2)−Cu(1)−S(1) (deg)	127.06(10)	N(2)−Cu(1)−N(3) (deg)	117.95(15)	124.16(8)
N(2)−Cu(1)−S(2) (deg)	102.83(10)	N(2)−Cu(1)−N(5) (deg)	114.49(14)	110.86(8)
S(1)−Cu(1)−S(2) (deg)	113.71(5)	N(3)−Cu(1)−N(5) (deg)	106.27(15)	107.46(8)
θ[b] (deg)	74.06	θ[b] (deg)	87.74	80.94

[a] Numbering scheme given in Figure 1. [b] θ is the angle between the two intersecting planes of the coordination tetrahedron: N(1)−Cu−N(2) and S(1)−Cu−S(2) for complex **7**, and N(1)−Cu−N(2) and N(3)−Cu−N(5) for complexes **8a** and **8b**, respectively.

throline copper(I) complexes, such as [Cu(dmp)$_2$]BPh_4 (202 pm)[32] or [Cu(dpdmp)$_2$]PF_6 (202−211 pm).[11] Despite the considerably rigid architecture of **5**, the rotational freedom of the aryl substituents in the 2- and 9-positions provides sufficient flexibility to adapt to the natural bonding distances of the copper center.

^{1}H NMR of Cu(bempp)PF_6 (7). The ^{1}H NMR data of **7** in $CDCl_3$ suggest that, in agreement with the solid-state structure, the complex adopts also a monomeric C_2-symmetric geometry in solution. The ligand architecture effectively prevents formation of oligo- or polymeric coordination complexes, which are characteristic for the coordination chemistry of monovalent copper with thioethers. Consistent with coordination of the thioether to the copper center, the benzylic CH_2 proton resonances are shifted to higher field by 0.6 and 1.08 ppm compared to the free ligand. Copper coordination renders the two benzylic protons chemically nonequivalent, resulting in an AM spin system with two doublets and significantly different chemical shifts (3.32 and 3.80 ppm). This observation indicates that dynamic exchange of the diastereotopic proton pair is slow on the NMR time scale at room temperature.

Crystal Structure of Cu(bpmpp)PF_6 (8a). Compared to complex **7**, the dihedral angle between the intersecting planes of N(1)−Cu−N(2) and N(3)−Cu−N(5) is substantially less twisted and approaches 87.7°, a nearly ideal tetrahedral geometry. The pyrazole substituent extends the chelate ring by an additional atom, which naturally leads to a different coordination geometry. The extension of the chelate ring to an eight-membered structure is also reflected in a slightly larger dihedral angle N(1)−C(1)−C(13)−C(18) and N(2)−C(10)−C(20)−C(25) between the phenanthroline ring plane and the aryl substituent. In complex **7** the two angles were measured to be 52.4° and 56.7° whereas in structure **8a** the analogous dihedral angles are 57.6° and 57.7°. The bond distances between copper and the phenanthroline nitrogens N(1) and N(2) are 205 and 206 pm, respectively, and are essentially identical compared to complex **7**. The copper pyrazole-nitrogen distances are slightly shorter with Cu−N(3) and Cu−N(5) equal 198 pm.

Crystal Structure of Cu(bdmpp)PF_6 (8b). Due to the steric requirements of the added methyl groups the coordina-

(32) Blake, A. J.; Hill, S. J.; Hubberstey, P.; Li, W. S. *J. Chem. Soc., Dalton Trans.* **1998**, 909.

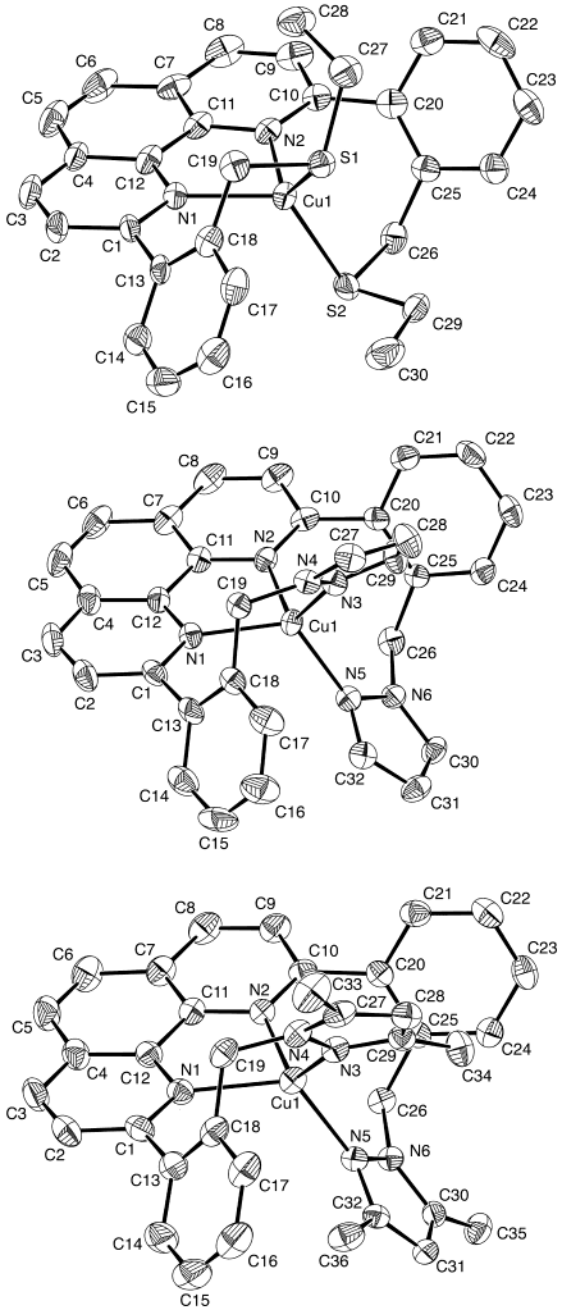

Figure 1. ORTEP plots and atom-numbering scheme for Cu(I) complexes **7** (top), **8a** (middle), and **8b** (bottom). Hydrogen atoms are omitted for clarity.

tion geometry of complex **8b** differs significantly from that of **8a**, despite the overall structural similarity. The dihedral angle between the intersecting coordination planes N(1)−Cu−N(2) and N(3)−Cu−N(5) of 80.9° is significantly flattened compared to **8a**. The steric demand of the methyl substituents is also reflected in longer bond distances of the coordination tetrahedron. The copper−nitrogen bond distances are generally increased by 3 to 12 pm. Interestingly, the deviation from an ideal C_2-symmetry is more pronounced in **8b** compared to the other two structures. The Cu−N(1) bond distance was determined to be 217 pm, whereas the symmetrical Cu−N(2) distance is only 209 pm. The space-filling representation depicted in Figure 2 illustrates how the

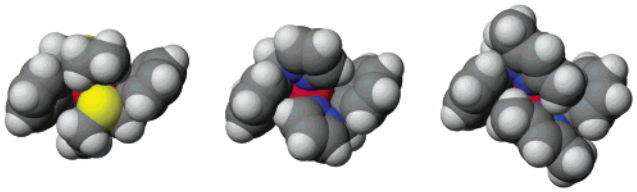

Figure 2. Space-filling representation for complex **7** (left), **8a** (middle), and **8b** (right).

coordination space around the copper center differs between the three complexes.

3. Photophysical Studies. 3.1. Steady-State Absorption and Emission. The spectroscopic properties of copper(I) phenanthroline complexes are dominated by low-lying metal-to-ligand charge-transfer excited states (MLCT), which give rise to characteristic charge-transfer absorption bands in the visible range.[7] In [1,10]phenanthroline two energetically close-lying π^* orbitals $a_2(\chi)$ and $b_1(\psi)$ act as electron acceptors upon excitation into the CT band (Figure 3).[33,34] The labels ψ (antisymmetric) and χ (symmetric) were introduced by Orgel and refer to the orbital symmetry with respect to the C_2 axis that passes through the ligand.[35]

As illustrated in Figure 3a the D_{2d}-symmetric coordination environment of copper(I) bis-phenanthroline complexes results in energetically degenerate d_{xz} and d_{yz} orbitals. Replacement of one of the phenanthroline ligands with a donor pair D leads to symmetry reduction and renders the two orbitals nondegenerate. In the resulting C_{2v}-symmetric environment almost all of the possible d $\rightarrow \pi^*$ electronic transitions are symmetry allowed. The only two exceptions are excitation into the LUMO (χ) from a d-orbital with a_1 symmetry ($d_{x^2-y^2}$ and d_{z^2}) and excitation into LUMO + 1 (ψ) from a d-orbital with b_2 symmetry (d_{yz}). Nevertheless, according to Day and Sanders the MLCT absorption intensity of C_{2v} symmetric [1,10]phenanthroline complexes is derived mainly from transitions that are polarized along the C_2 axis of the complex.[36] As shown in Figure 3 for an idealized C_{2v} symmetry, there are two such transitions possible, $b_1(\psi) \leftarrow d_{xz}$ and $a_2(\chi) \leftarrow d_{xy}$. In a twisted C_2-symmetric environment the previously mentioned symmetry-forbidden transitions are now all polarized along the C_2 axis. Given the higher energy expected for these transitions, a twisted coordination geometry will presumably alter only the blue edge of the MLCT absorption band. Apart from symmetry properties, the oscillator strength varies also with the degree of orbital overlap between the metal d and antibonding π^* ligand orbitals. The coefficients of the LUMO orbitals, in particular at the coordinating nitrogen atoms, are therefore of critical importance. Using both symmetry and orbital overlap as qualitative arguments, it is apparent that the $b_1(\psi) \leftarrow d_{xz}$ transition is favored over the $a_2(\chi) \leftarrow d_{xy}$ absorption (Figure 3a). The $b_1(\psi)$ orbital has indeed been identified by EPR spectroscopy as the predominant electron acceptor for a

(33) Phifer, C. C.; McMillin, D. R. *Inorg. Chem.* **1986**, *25*, 1329.
(34) Kaim, W. *J. Am. Chem. Soc.* **1982**, *104*, 3833.
(35) Orgel, L. E. *J. Chem. Soc.* **1961**, 3683.
(36) Day, P.; Sanders, N. *J. Chem. Soc. A* **1967**, 1530.

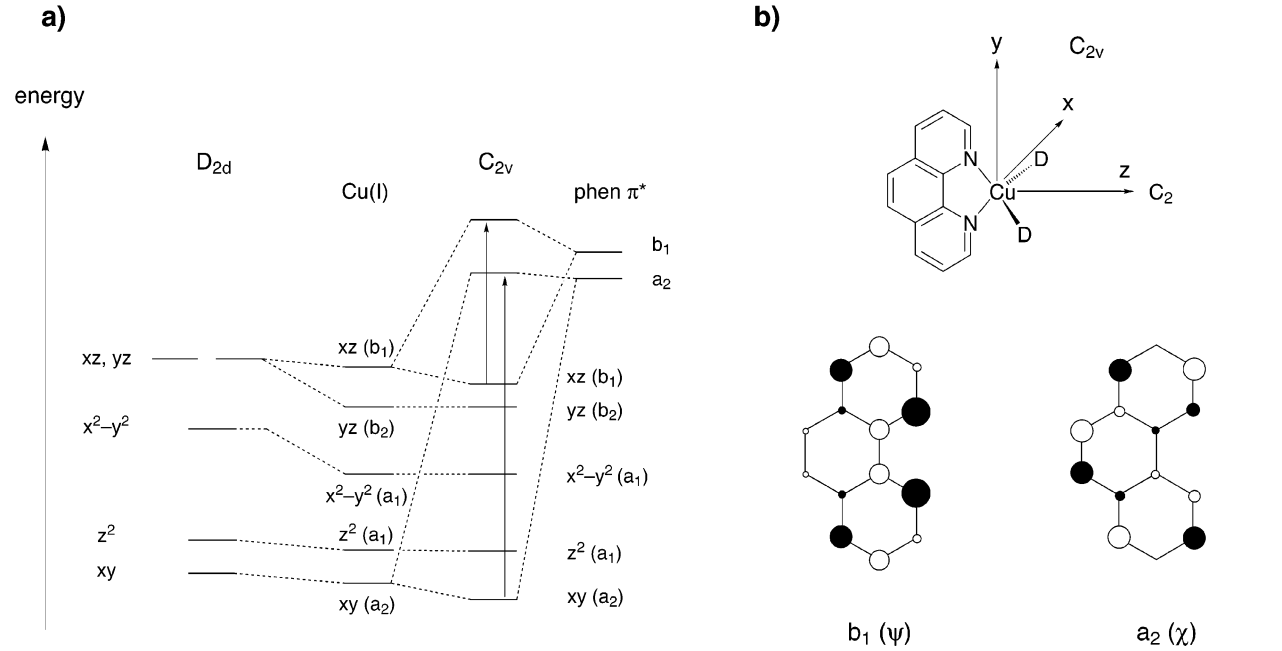

Figure 3. (a) Qualitative orbital energy diagram for Cu(I)−phenanthroline complexes with D_{2d} and C_{2v} symmetry. The arrows indicate transitions which are polarized along the C_2 axis (z coordinate). (b) Coefficients for the LUMO $a_2(\chi)$ and LUMO + 1 $b_1(\psi)$ of phenanthroline.

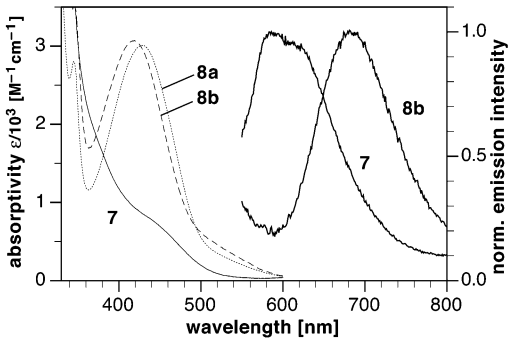

Figure 4. Charge-transfer (left) and normalized emission spectra (right) of complexes **7**, **8a**, and **8b** in dichloromethane at 25 °C. The (very weak) emission spectrum of **8a** has been omitted.

number of phenanthroline complexes with low-lying MLCT transitions.[34,37]

UV−Vis Spectra. The room-temperature charge-transfer absorption spectra for complexes **7**, **8a**, and **8b** in dichloromethane are shown in Figure 4. All relevant photophysical parameters including the ground-state oxidation potentials are compiled in Table 3. The two complexes **8a** and **8b** with the pyrazole-substituted ligands exhibit both strong CT absorptions over a broad range of the visible spectrum with a maximum centered around 428 and 418 nm, respectively. The molar absorptivity is very similar to the data reported for the 2,9-diphenyl-substituted phenanthroline copper(I) complex $[Cu(dpp)_2]^+$ and suggests a similar degree of electronic delocalization.[12] In the case of the structurally related bis-phenanthroline Cu(I) complexes the low-energy shoulder in the 550−600 nm range has been attributed to a geometrical distortion from D_{2d} symmetry.[38,39] As illustrated by the above symmetry analysis, the MLCT band is constituted of several possible transitions; however, flattening distortion to a C_2-symmetric environment is expected to induce changes in the blue edge of the MLCT band. Hence, the observed low-energy shoulders are consistent with both a C_{2v}- or C_2-symmetric coordination environment, and should not be mistaken as an indicator for dihedral distortion. The UV−vis absorption spectrum of **7** differs significantly from the spectra of the pyrazole-substituted complexes **8a** and **8b**. The MLCT absorption band appears only as a shoulder around 440 nm and with significantly smaller oscillator strength. The reason for this difference is not immediately apparent, but might be attributed to reduced orbital overlap due to the flattened coordination environment of **7**. Alternatively, the MLCT absorption might be shifted to higher energy and overlap with the strongly absorbing ligand-centered transitions.

Table 3. Electrochemical and Photophysical Data for Complexes **7**, **8a**, and **8b** in Dichloromethane[a]

data	**7**	**8a**	**8b**
$E_{1/2}$ (V)[b]	0.59 (85)	0.33 (65)	0.48 (69)
absorption λ_{max} (nm), ϵ (cm^{-1} M^{-1})[c]	440, shoulder (780)	428 (3010)	418 (3070)
emission[d] λ_{max} (nm)	585, 618 (shoulder)	700	685
quantum yield[e]	0.15%	0.004%	0.13%
lifetime (ns)	15, 155	5.2, 1.0, 0.09	110

[a] Measured at 25 °C. [b] Scan speed 100 mV s^{-1}, 0.1 M TBAP as electrolyte in nitrogen-saturated acetonitrile. The difference between anodic and cathodic current peak potential is given in parentheses (in mV). [c] Molar extinction coefficient in parentheses. [d] Excitation at 390 nm. [e] $Ru(bpy)_3(PF_6)_2$ as reference ($\Phi_f(H_2O) = 0.042$).[14]

Emission Spectra. Upon excitation at 390 nm complexes **8a** and **8b** exhibit a single broad emission band at 700 and 685 nm, respectively. The thioether derivative **7** emits at

(37) Farrell, I. R.; Hartl, F.; Zalis, S.; Mahabiersing, T.; Vlcek, A. *J. Chem. Soc., Dalton Trans.* **2000**, 4323.
(38) Klemens, F. K.; Palmer, C. E. A.; Rolland, S. M.; Fanwick, P. E.; McMillin, D. R.; Sauvage, J. P. *New J. Chem.* **1990**, *14*, 129.
(39) Ichinaga, A. K.; Kirchhoff, J. R.; McMillin, D. R.; Dietrich-Buchecker, C. O.; Marnot, P. A.; Sauvage, J. P. *Inorg. Chem.* **1987**, *26*, 4290.

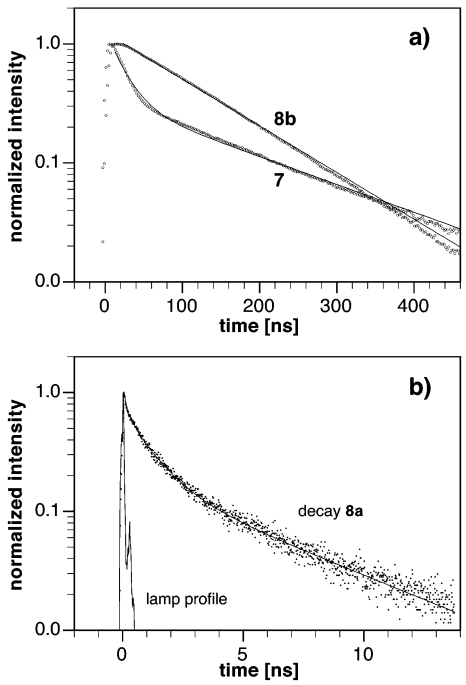

Figure 5. Luminescence decay data of complexes **7**, **8a**, and **8b** in degassed dichloromethane at 25 °C (time-correlated single photon counting).

considerably higher energy with a maximum at 585 nm and a shoulder around 618 nm (Figure 4). A detailed analysis of the emission spectra of copper(I) bis(phenanthroline) complexes by Kirchhoff et al. revealed that these complexes emit from close-lying, thermally equilibrated singlet and triplet excited states.[40] Quantum chemical calculations suggest a similar situation for the mono-phenanthroline complexes **7**, **8a**, and **8b** (section 4). The appearance of a single band does therefore not necessarily imply that emission occurs from a single excited state. Unlike compound **7** the emission maxima for **8a** and **8b** compare well with the peak emission of 690 nm reported for copper(I) bis(2,9-diphenylphenanthroline).[12] As shown for a series of structurally related copper(I) bis(phenanthroline) complexes, the emission energy reflects the extent of flattening distortion in the excited state. Upon increase of the steric requirements of the substituents in the 2- and 9-positions of the phenanthroline ring, the emission maxima are blue-shifted.[9,12,41] Differences in the flexibility of the ligand backbone might also be the key factor that leads to the higher emission energy of thioether derivative **7**. In fact, compound **7** contains a seven-membered chelate ring, whereas **8a** and **8b** comprise a larger eight-membered ring. The increased flexibility of **8a** and **8b** possibly allows a higher degree of flattening distortion in the Cu(II)-like excited state. This assumption is corroborated by the decrease of the emission quantum yield and excited-state lifetime (see below).

3.2. Time-Resolved Spectroscopy. As shown in Figure 5, the decay kinetics of complexes **7**, **8a**, and **8b** vary substantially. The thioether derivative **7** follows a biexponential decay law with short and long lifetime components of 15 and 155 ns, respectively. The emission of complex **8b** exhibits a slightly smaller lifetime of 110 ns, but follows a monoexponential decay law. The decay kinetics of complex **8a** is much faster and was fitted with a triexponential rate law yielding the lifetime components 5.2, 1.0, and 0.09 ns. In the discussion of photophysical properties it is often instructive to extract the radiative (k_r) and nonradiative (k_{nr}) decay rate from the quantum yield and the observed rate constant k_{obs}. The second- and third-order decay laws for **7** and **8a** imply that emission occurs from more than one excited state and therefore k_r and k_{nr} cannot be simply calculated. On a qualitative level the measured lifetimes parallel the trend in quantum yields.

According to detailed studies of copper(I) bis(phenanthroline) complexes, the shortening of the MLCT excited-state lifetime can be rationalized on the basis of energy gap law considerations or exciplex quenching with solvent molecules.[41−43] As previously noted, conformational locking by sterically demanding substituents restricts structural relaxation, induces a blue shift of the emission energy, and should increase the quantum yield as a consequence of the energy gap law. This prediction is based on the assumption that the vibrational overlap between the electronic ground and excited states is decreasing with increasing energy gap. This model is also helpful to rationalize the observed differences in the excited-state dynamics of **8a** and **8b**. The steric requirements of the methyl groups in **8b** not only reduce the conformational flexibility, but also restrict solvent access for exciplex quenching. As a result, the quantum yield and luminescence lifetime of **8b** are greatly improved compared to **8a**. The molecular architecture of complex **7** allows better solvent access, but is inherently less flexible due to the smaller size of the chelate ring. The resulting blue shift of the emission energy is in agreement with an increase in quantum yield and luminescence lifetime as predicted by the energy gap law.

Transient Absorption Spectra. Figure 6 depicts time-resolved absorbance-difference spectra for complexes **7**, **8a**, and **8b**. The samples were excited at 390 nm with a laser pulse of 120 fs duration and the spectra recorded with a "white-light" probe pulse at the indicated delay times. All three compounds exhibit a characteristic increase in absorption between 450 and 700 nm within 600 fs upon excitation. In contrast to previously reported transient absorption data for $Cu(dmp)_2^+$,[44,45] the shape and peak position of the spectrum change as a function of time. The data are therefore not consistent with a simple excited-state dynamics and suggest the consecutive formation of at least three different species. Since vibrational relaxation occurs on the picosecond time scale, the spectra observed during evolution of the signal

(40) Kirchhoff, J. R.; Gamache, R. E., Jr.; Blaskie, M. W.; Del Paggio, A. A.; Lengel, R. K.; McMillin, D. R. *Inorg. Chem.* **1983**, *22*, 2380.
(41) Cunningham, C. T.; Cunningham, K. L. H.; Michalec, J. F.; McMillin, D. R. *Inorg. Chem.* **1999**, *38*, 4388.
(42) Everly, R. M.; Ziessel, R.; Suffert, J.; McMillin, D. R. *Inorg. Chem.* **1991**, *30*, 559.
(43) Felder, D.; Nierengarten, J. F.; Barigelletti, F.; Ventura, B.; Armaroli, N. *J. Am. Chem. Soc.* **2001**, *123*, 6291.
(44) Palmer, C. E. A.; McMillin, D. R.; Kirmaier, C.; Holten, D. *Inorg. Chem.* **1987**, *26*, 3167.
(45) Chen, L. X.; Jennings, G.; Liu, T.; Gosztola, D. J.; Hessler, J. P.; Scaltrito, D. V.; Meyer, G. J. *J. Am. Chem. Soc.* **2002**, *124*, 10861.

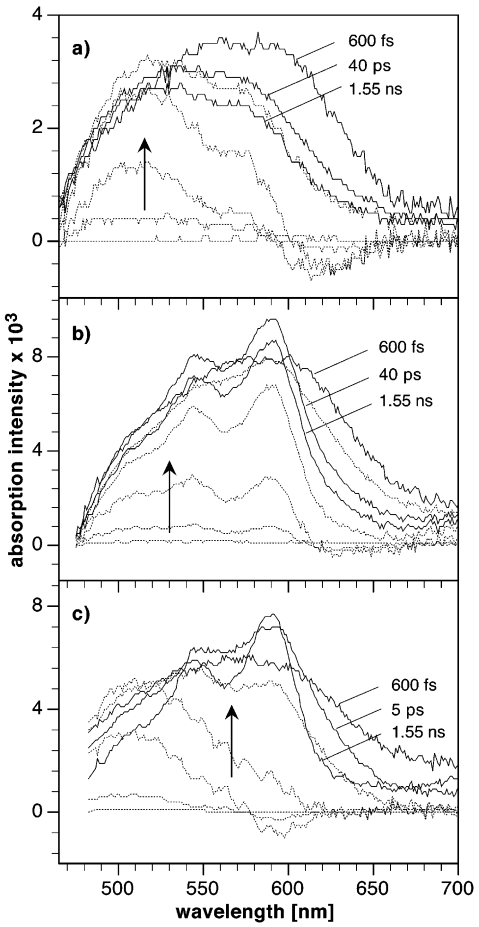

Figure 6. Room-temperature transient absorption spectra obtained after pulsed light excitation at 390 nm (0.8 mJ/cm^2, 120 fs fwhm) of (a) Cu(bempp)PF_6 (**7**), (b) Cu(bpmpp)PF_6 (**8a**), and (c) Cu(bdmpp)PF_6 (**8b**). The dotted spectra show the initial evolution of the signal with 0, 120, 240, 360, and 480 fs delay times.

(<500 fs) reflect only changes in the electronic structure. The initial spectra for compound **8a** and **8b** exhibit each a prominent signature with maxima at 540 and 590 nm (Figure 6b,c). The band shape resembles the ground state absorption spectrum of the phenanthroline radical anion with maxima at 585 and 636 nm, though with a significant blue shift. Time-resolved absorption studies with copper(I) bis(2,9-dimethylphenanthroline) showed qualitatively similar blue-shifted spectra, which were interpreted by the formation of the ligand radical anion in the excited state.[44,45] Interestingly, after 40 ps the two maxima coalesce to a single broad band, which again disappears to form a qualitatively similar spectrum compared to the one observed within the first 500 fs. The transient absorption spectra series for complex **7** shows qualitatively the same pattern (Figure 6a). The initial spectra also exhibit two maxima at 520 and 570 nm, which are slightly more blue-shifted compared to **8a** and **8b**. As observed previously for the pyrazole derivatives **8a** and **8b**, the two maxima become gradually broader and again yield the original band shape after about 1 ns. In summary, the data strongly support the formation of the ligand radical anion in the excited state and show qualitatively a very similar trend for all three complexes **7**, **8a**, and **8b**. The temporary spectral broadening is presumably due to vibrational relaxation during the flattening process followed by structural adjustments for the reduced ligand and possibly formation of a five-coordinate species.[45]

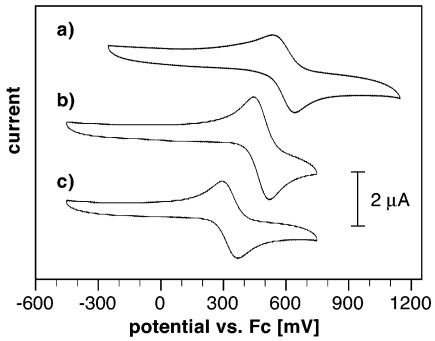

Figure 7. Cyclovoltammogram for complexes **7** (a), **8a** (c), and **8b** (b) in acetonitrile with 0.1 M Bu_4NPF_6 as supporting electrolyte, glassy carbon electrode, and Ag/Ag^+ reference electrode (potential plotted against Fc/Fc^+ couple).

3.3. Redox Properties. Cyclic voltammetry studies of complexes **7**, **8a**, and **8b** in acetonitrile reveal for all compounds a quasi-reversible one-electron oxidation−reduction wave associated with the Cu(I)/Cu(II) couple (Figure 7). The measured half-wave potentials range between 0.33 and 0.59 V (vs Fc/Fc^+) and indicate significant stabilization of the monovalent oxidation state (Table 3). A comparison with published half-wave potentials of substituted bis-phenanthroline complexes suggests that the rigid molecular architecture of **7**, **8a**, and **8b** yields a comparable stabilization. For example, $Cu(dmp)_2^+$ (dmp = 2,9-dimethylphenanthroline) is oxidized at $E = 0.27$ V (vs Fc/Fc^+)[9] whereas the potential of the sterically more crowded complex $Cu(dpp)_2^+$ (dpp = 2,9-diphenylphenanthroline) was measured to be $E = 0.32$ V (vs Fc/Fc^+).[12] The significantly greater potential observed for complex **7** can be attributed to the different coordination environment. The replacement of a nitrogen donor atom with a sulfur has been shown to significantly reduce the affinity toward Cu(II),[46] and therefore the Cu(I)/Cu(II) redox couple is shifted to a more positive potential. In contrast, complex **8a** and **8b** have the same set of donor atoms, and the potential difference of 0.15 V is primarily due to differences in the ligand architecture. Copper(II) complexes with diimine ligands have a high tendency to form five-coordinate complexes in solution, typically via coordination of a solvent molecule as the fifth ligand.[11] Steric shielding by the four methyl substituents in **8b** reduces solvent accessibility and therefore destabilizes the Cu(II) oxidation state. Solvent coordination in the Cu(II) state is additionally supported by the larger than expected potential difference between the oxidation and reduction peaks. For all complexes the differences are significantly higher than the 56.5 mV expected for a perfectly reversible redox process (Table 3). Structural rearrangements followed by coordination of a solvent molecule between the oxidation and reduction steps may well account for this observation.

(46) Ambundo, E. A.; Deydier, M.-V.; Grall, A. J.; Aguera-Vega, N.; Dressel, L. T.; Cooper, T. H.; Heeg, M. J.; Ochrymowycz, L. A.; Rorabacher, D. B. *Inorg. Chem.* **1999**, *38*, 4233.

Table 4. Calculated Structural Parameters for Cu(I) Complexes **7**, **8a**, and **8b**[a]

[Cu(bempp)]$^+$ (**7**)		[Cu(bpmpp)]$^+$ (**8a**)	[Cu(bdmpp)]$^+$ (**8b**)
Cu(1)−N(1) (Å)	2.014	Cu(1)−N(1) (Å)	2.040	2.081
Cu(1)−N(2) (Å)	2.000	Cu(1)−N(2) (Å)	2.044	2.089
Cu(1)−S(1) (Å)	2.270	Cu(1)−N(3) (Å)	1.985	2.018
Cu(1)−S(2) (Å)	2.298	Cu(1)−N(5) (Å)	1.987	2.022
N(1)−Cu(1)−N(2) (deg)	84.6	N(1)−Cu(1)−N(2) (deg)	82.2	81.0
N(1)−Cu(1)−S(1) (deg)	107.0	N(1)−Cu(1)−N(3) (deg)	116.0	113.4
N(1)−Cu(1)−S(2) (deg)	122.0	N(1)−Cu(1)−N(5) (deg)	119.4	121.7
N(2)−Cu(1)−S(1) (deg)	128.3	N(2)−Cu(1)−N(3) (deg)	119.5	122.1
N(2)−Cu(1)−S(2) (deg)	103.1	N(2)−Cu(1)−N(5) (deg)	115.7	113.1
S(1)−Cu(1)−S(2) (deg)	111.1	N(3)−Cu(1)−N(5) (deg)	104.0	105.2
θ[b] (deg)	73.5	θ[b] (deg)	87.0	82.6

[a] B3LYP/6-31G** optimized geometries, with numbering scheme given in Figure 1. [b] θ is the angle between the two intersecting planes of the coordination tetrahedron: N(1)−Cu−N(2) and S(1)−Cu−S(2) for complex **7**, and N(1)−Cu−N(2) and N(3)−Cu−N(5) for complexes **8a** and **8b**, respectively.

4. Quantum Chemical Calculations. 4.1. Ground-State Geometries. Geometries obtained by optimization at the B3LYP/6-31G** level of theory are presented in Table 4. In general, there is good agreement with the observed X-ray structures in Table 2. Distances between Cu and the coordinating atoms are generally within 0.04 Å of experiment; this compares to an average error of 0.013 Å at this level of theory[47] for bonds in the G2 data set,[48] which contains primarily covalent bonds between first-row atoms. The somewhat larger discrepancies in this case seem reasonable given that the distances are larger and correspond to weaker binding than in the G2 molecules, and they are smaller than errors (0.09 Å) in predicted distances for tetracoordinated Cu(I) in $[Cu_2(pip)_2]$ [pip = (2-picolyliminomethyl)pyrrole anion] using B3LYP/LANL2DZ.[49] Bond angles are within 3° (compared to an average error of 0.6° for the G2 molecules), and the angle between coordinating planes is predicted within 2° of the experimental value. These results indicate that there are no major distortions in the coordination geometry due to crystal packing forces or the influence of the counterion.

The experimental results indicate a slight distortion from local C_2 symmetry, as seen by the differences in the distance to Cu of N(1) and N(2) [or N(3) and N(5), or S(1) and S(2)]. The theoretical results are also consistent with this distortion, although the difference in bond lengths is generally reduced. The most significant distortion is a 0.078 Å difference between the distances to N(1) and N(2) in **8b**, while this difference is only 0.008 Å theoretically. The crystal structures were used as starting geometries during optimization, and it is possible that the potential energy surface is sufficiently flat that the optimization criteria (maximum gradient 0.0003 hartree/bohr, energy change 10^{-6} hartree) may be satisfied before the precise minimum geometry, which might be symmetric, has been reached. This seems likely for **8a** and **8b**, where the distortion in the theoretical geometry is only a few thousandths of an angstrom. The difference is larger in **7**, probably because of the different orientations of the two pendant ethyl groups observed in the crystal structure and retained in the theoretical geometry.

4.2. TD-DFT Calculations of Excited States. To understand the electronic spectrum of complexes **7**, **8a**, and **8b** in more detail, vertical excitation energies were computed using time-dependent density functional theory (TD-DFT), again with the B3LYP functional and 6-31G** basis set. A large number of singlet and triplet states are predicted between 1.7 and 4 eV, and the calculated excitation energies, oscillator strengths, and approximate composition of these states are tabulated in the Supporting Information. In general, TD-DFT is a fairly reliable and inexpensive technique, yielding excitation energies for valence states with a typical accuracy of about 0.4 eV.[23,24] Previous applications of TD-DFT to vertical spectra of transition metal complexes indicate that energies of charge-transfer states are typically underestimated by several tenths of an electronvolt,[37,50] while Tozer et al.[51] have shown that these errors can grow to 1 eV or more for certain cases. One very recent study indicates that B3LYP TD-DFT succeeds in accurately modeling the photophysics of $[Cu(I)(dmp)_2]^+$.[52] Our goals in the present study are to obtain a qualitative picture of the excited states and to evaluate the performance of TD-DFT for this case.

The observed λ_{max} values for absorption of **7**, **8a**, and **8b** (Table 3) are 440 nm (2.82 eV), 428 nm (2.90 eV), and 418 nm (2.97 eV). The observed excitation energies are reasonably well matched by the TD-DFT predictions, which are depicted schematically in Figure 8 for vertical singlet and triplet transition energies. The excited singlet states with the largest oscillator strengths are at 2.57 (**8a**, strength 0.065), 2.48 (**8b**, strength 0.047), and two near-degenerate states for **7** at 2.79 and 2.83 eV (strength 0.032). For **8a** and **8b**, the excited-state energy is underestimated as expected for charge-transfer states at this level of theory. For **7**, the agreement with experiment appears fortuitously good. However, it is possible that this state is also theoretically underestimated if the MLCT is not the shoulder assigned in Figure 4 but instead is buried within the higher-energy transitions below 400 nm.

(47) Bauschlicher, C. W. *Chem. Phys. Lett.* **1995**, *246*, 40.
(48) Curtiss, L. A.; Raghavachari, K.; Trucks, G. W.; Pople, J. A. *J. Chem. Phys.* **1991**, *94*, 7221.
(49) Liao, Y.; Novoa, J. J.; Arif, A.; Miller, J. S. *Chem. Commun.* **2002**, 3008.
(50) Full, J.; Gonzalez, L.; Daniel, C. *J. Phys. Chem. A* **2001**, *105*, 184.
(51) Tozer, D. J.; Amos, R. D.; Handy, N. C.; Roos, B. O.; Serrano-Andres, L. *Mol. Phys.* **1999**, *97*, 859.
(52) Zgierski, M. Z. *J. Chem. Phys.* **2003**, *118*, 4045.

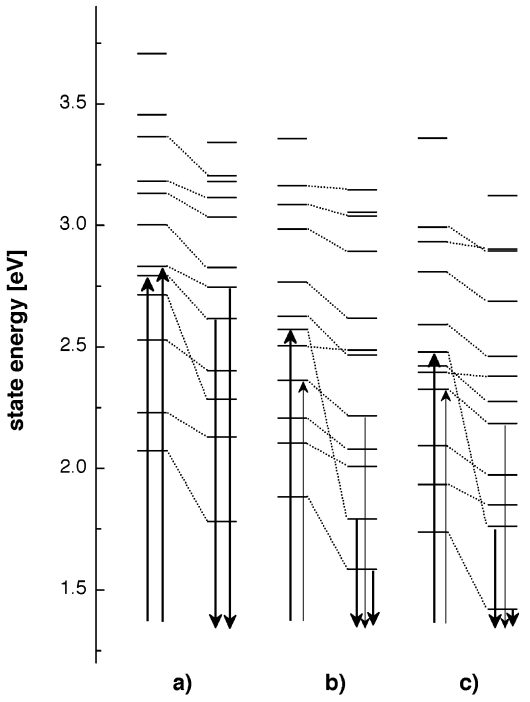

Figure 8. Energy level diagram of the calculated singlet (left) and triplet (right) excited states for **7** (a), **8a** (b), and **8b** (c) (TD-DFT B3LYP/6-31G**).

The nature of the low-lying excited states can be elucidated by the electron attachment and detachment analysis of Head-Gordon and co-workers.[25] This procedure decomposes the difference density between ground and excited states into the negative of a "detachment density" corresponding to the removal of charge from the ground state plus an "attachment density" corresponding to the new arrangement of this charge in the excited state. The attachment/detachment density plots for the lowest seven excited states of **7**, **8a**, and **8b** are presented in Figure 9. The plots are very similar among the molecules considered, and they clearly indicate that all of the lowest-lying states are MLCT states in which electron density is detached from Cu and attached onto the phenanthroline moiety. In some cases (particularly for **7**) a minor amount of density is also removed from some of the atoms in closest proximity to Cu. In nearly all of the lowest-lying singlet states, the electron attachment density is consistent with either the $b_1(\psi)$ or $a_2(\chi)$ phenanthroline π^* orbitals, which are very close energetically (within 0.001 hartree for the three molecules considered). The rest of the ligand serves primarily as a scaffold to arrange approximate tetrahedral coordination in the ground state and does not participate directly in the vertical electronic excitation process.

For the states predicted to be the strongest absorbers in **8a** and **8b** (S_6 and S_7, respectively), the attachment/detachment density analysis suggests the promotion of an electron from a d_{xz} orbital to the phenanthroline $b_1(\psi)$ π^* orbital. As described in section 3.1, this is expected to be the strongest MLCT transition because it should feature the best orbital overlap between the two orbitals involved in the transition. Moreover, the computed transition moment lies primarily along the approximate C_2 axis, which is again consistent with the general rule that the primary intensity of

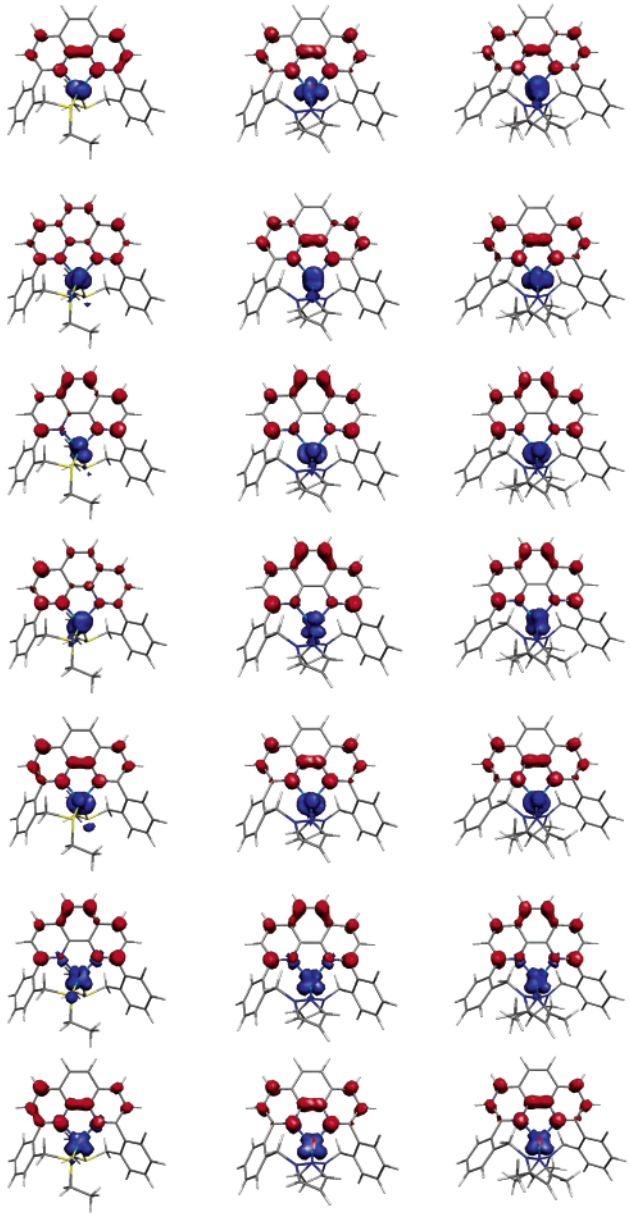

Figure 9. Attachment/detachment densities for the seven lowest excited states of **7** (left), **8a** (middle), and **8b** (right). Plots are arranged with increasing energy from bottom to top (TD-DFT B3LYP/6-31G**).

MLCT absorption in such complexes arises from transitions polarized in the same direction as the charge transfer.[36] The second most intense absorbing state in **8a** and **8b** is the S_4 state, which looks qualitatively like a d_{xz} to phenanthroline $a_2(\chi)$ π^* transition and is polarized primarily along the y axis. Results for **7** are similar, although the electron attachment density for the two most intensely absorbing states (S_4 and S_6) mixes the near-degenerate unoccupied $b_1(\psi)$ and $a_2(\chi)$ phenanthroline orbitals. The detachment density likewise shows some d orbital mixing. The reduced intensity of the strongest transition in **7** compared to **8a** and **8b** seems consistent with a reduction in orbital overlap caused by the larger deviation from a tetrahedral coordinating geometry.

The TD-DFT computations reveal a dense manifold of low-lying triplet states, similar to the singlet manifold (see Figure 8). It is therefore challenging to assign the emission

spectrum, since any of these states are potentially emissive; indeed, the time-resolved spectra discussed above already indicate emission from multiple states for **7** and **8a**. At the ground-state geometry, the lowest-lying triplet states are at 1.78 (**7**, expt 2.12), 1.59 (**8a**, expt 1.77), and 1.42 eV (**8a**, expt 1.81). These energies are roughly consistent with the observed λ_{max} values for emission for the given level of theory, but such a comparison neglects geometry relaxation effects in the excited state which will reduce the energy gap. To attempt to estimate the effect of geometry relaxation, B3LYP/6-31G** optimizations were performed for the lowest-lying triplets of each complex. The vertical emission energies from this lowest triplet, computed as the energy difference between the B3LYP energies for the triplet and singlet at the triplet geometries, took on much lower values of 1.1−1.3 eV. This suggests that either there is a fundamental difficulty of B3LYP for computing vertical singlet−triplet gaps for charge-transfer states or most emission is taking place from higher-lying triplets and/or before geometry relaxation is completed.

Conclusions

The detailed structural and spectroscopic characterization of a series of geometrically constrained Cu(I) phenanthroline complexes revealed a picture that strongly resembles the photophysics of related and well-investigated copper(I) bis-phenathroline complexes. The rigid ligand architecture of the studied complexes provides significant stabilization to restrict structural relaxation in the excited state. Thus, the observed emission lifetimes and quantum yields compare well with the structurally related bis-phenanthroline complexes. However, transient absorption data and electrochemical measurements both indicate that coordinative rearrangements occur in the excited state leading to nonradiative deactivation via exciplex quenching. Conformational constraints combined with suppression of exciplex quenching are both key elements to enhance the emission energy, extend the emission lifetime, and improve the quantum yield.[41] McMillin and co-workers have recently demonstrated that this strategy leads to highly emissive Cu(I) complexes with very impressive quantum yields of up to 16%.[53,54] By increasing the size of the aryl substituent similar enhancements might be possible for the investigated complexes with 1:1 binding stoichiometry.

Acknowledgment. Financial support from the Georgia Institute of Technology is gratefully acknowledged. C.D.S. acknowledges support by the National Science Foundation through Grant CHE-0091380, and A.G. was supported by the Georgia Institute of Technology's Faculty Development Program and NSF Grant 9974841. Computations were supported by the Center for Computational Molecular Science and Technology at the Georgia Institute of Technology and partially funded through a Shared University Research (SUR) grant from IBM and the Georgia Institute of Technology. We also thank Sarah Shealy and David Bostwick for mass spectral data, and Dr. Mira Jasowicz for her support with the electrochemical measurements.

Supporting Information Available: X-ray structural acquisition and analysis (CIF) and additional information as mentioned in the text. This material is available free of charge via the Internet at http://pubs.acs.org. The crystallographic data for the structural analyses have been deposited with the Cambridge Crystallographic Data Centre (deposition numbers CCDC 213571-213573). Copies of this information may be also obtained free of charge from The Director, CCDC, 12 Union Road, Cambridge CB21EZ, U.K. (fax, +44-1223-336033; e-mail, deposit@ccdc.cam.ac.uk or http://www.ccdc.cam.ac.uk).

IC034529J

(53) Cuttell, D. G.; Kuang, S. M.; Fanwick, P. E.; McMillin, D. R.; Walton, R. A. *J. Am. Chem. Soc.* **2002**, *124*, 6.
(54) Kuang, S. M.; Cuttell, D. G.; McMillin, D. R.; Fanwick, P. E.; Walton, R. A. *Inorg. Chem.* **2002**, *41*, 3313.